Investigation of the wake energy recovery of cross-flow turbines in paired configuration by means of 3d-CFD and analysis of the streamwise momentum budget

Stefania Zanforlin[*] and *Paola* Lupi

Dipartimento di Ingegneria dell'Energia, dei Sistemi, del Territorio e delle Costruzioni (DESTEC), Università di Pisa, largo L. Lazzarino 1, 56122 Pisa, Italy

Abstract. Literature suggests that cross-flow turbines (CFTs) could be suitable for off-shore wind farms because of the high power-density achievable by shortening the distance between arrays as allowed by a fast wake energy recovery experimentally detectable. By means of 3d-CFD, we analysed the effect of the rotation verse of CFTs in counter-rotating paired configuration on the wake behaviour. Then, we applied the momentum-budget approach to identify the fluid dynamic mechanisms which are more effective in supporting the streamwise momentum recovery. The following results are found. (A) The counter-rotating vortices occurring in the near-wake as a consequence of the vortex shedding at the blade tip are responsible for the vertical advection that enters high momentum flow inside the wake. (B) The turbulent transport contribution is less important, yet it becomes significant starting from the medium wake. (C) For the inner-downwind layout the wake shape appears similar to that of a single turbine, whereas for the inner-upwind layout it is greatly contracted in horizontal direction and enlarged in vertical direction (D). The momentum recovery appears slightly more delayed than in case of a single turbine, yet the velocity deficit appears less extensive for the inner upwind layout that, especially thanks to the wake lateral contraction, could be the preferable in farms consisting in staggered arrays, allowing to shorten the lateral distance between adjacent pairs.

1 Introduction

Cross-flow turbines (CFTs) can be considered a valid alternative to horizontal axis turbines (HATs) for off-shore wind applications thanks to constructive simplicity and ability to work independently of flow direction. Moreover, by adopting floating platforms further advantages can be achieved: greater stability, since the centre of gravity is much lower than in HATs, that can help reduce the platform costs [1,2], and the platform motion would just negligibly affect energy output as CFTs still exhibit good performance in skewed flow [3,4]. On the other hand, CFTs are penalized by low starting-torque and lower efficiency than

---

[*] Corresponding author: stefania.zanforlin@unipi.it

HATs. Yet, the strong point of CFTs which would more than compensate for the lower efficiency of the single device, is the higher power density achievable with multi-device arrangements, i.e. the possibility of generating an energy greater amount from a sea limited area. To this end, two strategies are viable. The first is to adopt pairs of closely-spaced counter-rotating turbines, that can exploit beneficial fluid dynamic interactions [5-7]. The mechanisms that determine a power increase with respect to isolated turbines are described in [8, 9]: turbine blockage that entails flow acceleration outside of the turbines and inside the aisles between adjacent turbines; more favourable direction of the flow approaching the blade during upwind path; wake contraction, that increases the torque generation during the downwind path. However, to date there are only 2d CFD analyses so it is not known how the close proximity of turbines affects 3d phenomena such as blade tip losses or the wake characteristics. The second strategy to improve power density is shortening the distance between arrays, as allowed by a fast energy recovery experimentally measured by Kinzel *et al.* [6] in the wakes of a CFT cluster. Therefore, to plan efficient farm layouts it is important to know in depth the energy recovery mechanisms of the wake and to understand which operating and turbine geometrical parameters can support them. At now, only few studies can be found in literature on this subject. The experimental investigations by Bachant and Wosnik [10] and Rolin and Porté-Agel [11] on the 3d-character of straight-bladed CFT wakes have shown that the vertical advection induced downstream the rotor by pairs of counter-rotating vortices occurring at the turbine top and bottom sides plays a dominant role in the wake dynamics by entraining faster fluid from the freestream and therefore by supporting an extraordinary wake recovery that makes CFT wakes much shorter than HAT wakes. These vortex pairs are deemed the consequence and evolution of the vortex shedding occurring at the blade tips, although they are visible even in case the blade tips are closed by plates, as observed by Ryan *et al.* [12] who also tested the role of Tip Speed Ratio (*TSR*, defined as $R*\Omega/U_0$, where R is the turbine radius, Ω is the rotational speed, and U_0 is the free stream velocity) finding that the strength of the vortices increases with *TSR*. Recently Zanforlin and Lupi [13], by means of a CFD investigation, have found that turbines with high solidity and cambered-out blade profile exhibit strong tip vortices and fast wake recovery. The only study dealing with the wake complete evolution of a pair of side-by-side closely spaced turbines is the experimental investigation by Vergaerde *et al.* [14], who detected the wake main characteristics up to 12 diameters downstream the shaft demonstrating that different directions of rotation of paired CFTs induce very different wakes.

To understand the energy recovery process of the wake in a comprehensive way, it is possible to combine the direct observation of the main variables of the flow field (velocity and turbulence components) obtainable from experimentation or CFD with an analysis based on the momentum budget approach, which allows to quantify the role of advection and turbulent and viscous transport in the replenishment of the streamwise momentum deficit. In addition to Bachant and Wosnik [10] and Rolin and Porté-Agel [11], momentum budget analyses can be also found in the experimental study by Ouro *et al.* [15] on a Gorlov-type CFT, and in the Large Eddy Simulation (LES) study by Posa [16], despite this last study does not allow to consider vertical advection due to the 2.5d nature of the CFD simulations. Some common trends are observable in those studies: in the near-wake the dominant mechanisms are vertical (positive contribution) and lateral (negative contribution) advections whereas turbulent transport is much less and becomes important only in the medium-far wake. However, all the aforementioned momentum budget analyses treat with a single turbine.

In the present investigation, for the first time by means 3d CFD, we analyse the 3d fluid dynamic phenomena occurring in a pair of counter-rotating turbines to understand if a close proximity influences the blade tip losses and, above all, if it supports or delays the energy recovery of the wakes. To this end, we combine qualitative observations of the flow field with a momentum budget analysis.

2 Methodology

In this section the validation of the CFD model is presented in comparison to experimental velocity profiles in the wake of a CFT found in literature. Next, the fundamentals of the momentum budget analysis and details of the methodology we adopted to calculate the terms appearing in the equation are described.

2.1 Set-up and validation of the CFD model

For both the validation and the main simulations of this study we adopted the same turbine experimentally investigated by Vergaerde *et al.* [14]. We have chosen this bibliographic reference since it shows results of the wake behaviour for an isolated CFT and also for pairs of counter-rotating CFTs, moreover, thanks to the very large test section of the wind tunnel, any blockage effect is avoided. The rotor main characteristics are: diameter, D, of 0.5m; two straight NACA0018 blades; blade vertical span, H, of 0.8m; blade chord, c, of 0.05m. As in [14], for all our simulations the operating free stream speed, U_0, is 10.7 m/s, and *TSR* is 3.

ANSYS-ICEM has been used to generate the multi-block structured 3d grids, with the addition of O-grids to thicken the distribution of cells in the areas of greatest interest and, at the same time, to improve their quality. Two grid levels are used to simulate the blade rotation via the sliding mesh method: a fixed sub-grid with the outer dimensions of the flow domain and a rotating sub-grid including the turbine blades. All around the blades the grid is very fine to make sure that $y+$ at the walls stay below 0.4, following the work of Maître *et al.* [17], who analysed the effect of $y+$ realizing that averaged $y+>1$ causes a pressure drag overestimation in turbines exposed to significant flow separation. The moving and the fixed domains are joined together by means of a boundary condition (BC) of interface. The other BC are: velocity inlet for the inlet face; pressure outlet for the exit; symmetry for the top boundary that corresponds to the ceiling of the test-chamber (this simplification, respect to the "wall" condition, is justified by the distance between ceiling and turbine); wall for the bottom in case of the validation task (since it corresponds to the wind tunnel floor) or symmetry for the main simulations of this paper (since only half blade length is simulated to save computation time). Some grid details are shown in Fig. 1, where the dashed magenta circumference delimitates the rotating grid.
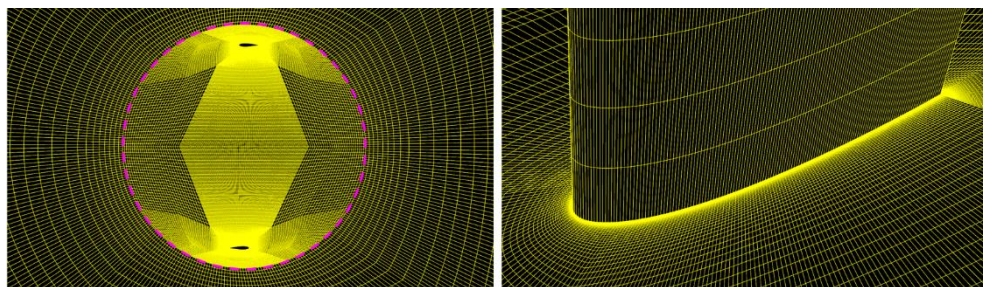

Fig. 1. (left) Grid on the horizontal plane passing through the mid-span of the blades; (right) grid detail in the blade region at the intersection between the blade and the mid-span plane.

The simulations are performed using ANSYS-Fluent v19. To model the turbulence, the k-ω SST (Shear Stress Transport) is adopted [18, 19]; this model is widely used in the simulation of wind and tidal CFTs since it is considered well appropriate in case of flow characterised by strong adverse pressure as happens in CFTs, especially when operating at low *TSR*. The algorithm for the velocity-pressure coupling is SIMPLEC. About the spatial discretization scheme, the Least Squares Cell-Based (LSCB) is set for gradient; pressure

interpolation, turbulent kinetic energy and specific dissipation rate formulations are based on second order schemes. Temporal discretization is also based on a second order implicit method. The convergence criteria for each time-step is 1×10^{-4} for the residuals of continuity, velocity components, turbulence kinetic energy and specific dissipation rate. When using a sliding mesh, to obtain a satisfactory numeric convergence the time-step should not be larger than the time required for advance the mobile interface by a distance corresponding to one cell thus, in order to consider the smallest cell at the interface, a time-step corresponding to 0.5° of revolution is adopted; this value is also in accordance with Balduzzi *et al.* [20].

Since our work is focused on the wake dynamics, the reliability of the overall CFD model has been verified versus the wake experimental profiles reported in [14] for the single turbine. For the validation task the entire blade length has been simulated, adopting domain dimensions corresponding to the dimensions of the test chamber (for the details of which, please refer to [14]). Due to the enormous computation times required to simulate many revolutions in an extended domain made up of millions of cells, the sensitivity analysis at the fineness of the grid was not carried out. However, we have chosen the model settings recommended by the best practice present in the literature (such as the aforementioned *y+*) and a grid that throughout the development of the wake is made of very small and very regular cells (rectangular parallelepipeds). Fig. 2 shows horizontal profiles of U/U_0 (where U is the streamwise velocity) achieved with CFD at various locations along x-axis (normalised by D) downstream the rotor; the *z*-coordinate corresponds to the blade midspan. Left in the figure, the sensitivity of the results to the number of revolutions is reported; it can be seen that for the near and medium wake (until *x/D*=6) it is sufficient to simulate 18 revolutions, whereas at *x/D*=8 the wake needs at least 21 revolutions to be considered completely developed. A sufficient agreement is found by the comparison between the CFD results achieved after 18 revolutions and the experimental measurements, as shown right in Fig. 2.
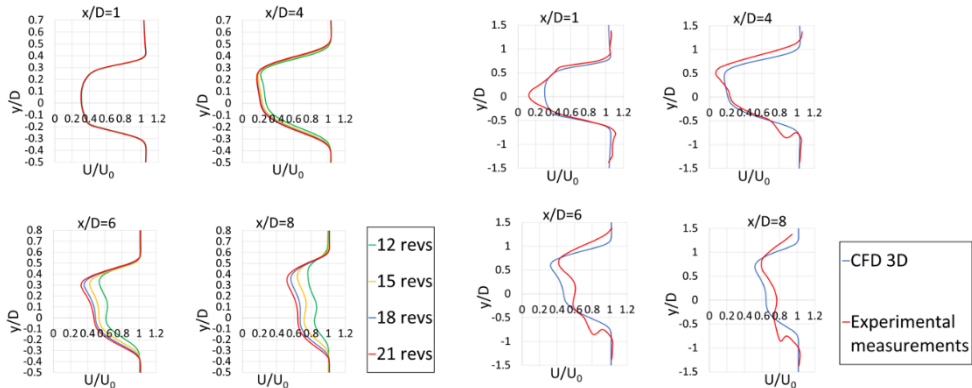

Fig. 2. Streamwise velocity profiles achieved by CFD at different *x*-locations: (left) effect of revolution number; (right) comparison with experimental data from Vergaerde *et al.* [14].

2.2 Momentum budget approach

To find the physical mechanisms that mostly favour the wake recovery, the streamwise Reynolds Averaged Navier-Stokes (RANS) momentum equation is rearranged as in Bachant and Wosnik [10] and Ouro *et al.* [15], with the assumptions of steadiness and incompressibility of the flow:

$$\frac{\partial \overline{U}}{\partial x} = -\frac{\overline{V}}{\overline{U}}\frac{\partial \overline{U}}{\partial y} - \frac{\overline{W}}{\overline{U}}\frac{\partial \overline{U}}{\partial z} - \frac{1}{\rho \cdot \overline{U}}\frac{\partial \overline{P}}{\partial x} - \frac{1}{\overline{U}}\frac{\partial}{\partial x}\overline{U'U'} - \frac{1}{\overline{U}}\frac{\partial}{\partial y}\overline{U'V'} - \frac{1}{\overline{U}}\frac{\partial}{\partial z}\overline{V'W'}$$

$$+ \frac{\nu}{\overline{U}}\left(\frac{\partial^2 \overline{U}}{\partial x^2} + \frac{\partial^2 \overline{U}}{\partial y^2} + \frac{\partial^2 \overline{U}}{\partial z^2}\right) \tag{1}$$

The physical meaning of all terms on the right hand of Eq. (1) is specified in Table 1: lateral and vertical advection, streamwise pressure gradient, three terms of turbulent transport (x, y and z derivatives of the Reynolds stresses), viscous diffusion.

Table 1: Terms used to compute contributions to streamwise momentum recovery

y advection	$-\overline{V}/\overline{U} \cdot (\partial \overline{U}/\partial y)$
z advection	$-\overline{W}/\overline{U} \cdot (\partial \overline{U}/\partial z)$
pressure transport	$-(1/\rho \cdot \overline{U}) \cdot (\partial \overline{P}/\partial x)$
x turbulent transport	$-1/\overline{U} \cdot (\partial \overline{U'U'}/\partial x)$
y turbulent transport	$-1/\overline{U} \cdot (\partial \overline{U'V'}/\partial y)$
z turbulent transport	$-1/\overline{U} \cdot (\partial \overline{U'W'}/\partial z)$
viscous diffusion	$\nu/\overline{U} \cdot (\partial^2 \overline{U}/\partial x^2 + \partial^2 \overline{U}/\partial y^2 + \partial^2 \overline{U}/\partial z^2)$

All terms are normalized by D/U_0, and spatially averaged over cross-sections placed at various distances downstream the rotor, yet limiting the averaging operation to the wake portion contained within the velocity magnitude iso-contour corresponding to U_0, as done by Posa [16]. The contributions to streamwise momentum recovery were obtained using the time-average values of the flow field achieved during the last two turbine revolutions (that are the 21st and 22nd). It should be observed that a first advantage of CFD is the possibility to calculate all the terms appearing in Eq. (1), whereas in experimental tests this would be technically difficult or very expensive. For instance, the contributions of the streamwise pressure gradient and the streamwise turbulent transport were not computed by Bachant and Wosnik [10] and Ouro *et al.* [15] due to the objective difficulty to obtain gradients; furthermore, in [10] the contribution of streamwise derivative of the viscous stresses was not computed, while in [15] the viscous diffusion was assumed negligible and then it was omitted. Another advantage of CFD is to be able to use very small computation cells, which leads to finer resolution than in experimental works for the terms in Eq. (1). Our grid, in the wake region, starting from $2D$ downstream the turbine axis and up to the domain outlet, is made of cells with uniform spacing along x, y and z equal to: $0.43c$, $0.35c$ and $0.28c$.

3 Results

In this section the two configurations assumed for the paired CFTs are defined, and the differences between the blade tip losses predicted for the paired turbines and those predicted for the single turbine are discussed. Then, after a brief discussion on the origin of the large vortical structures occurring in the near-wake, the wake momentum replenishment will be analysed on cross-sectional planes set along the wake, first qualitatively by observing the flow field velocity, then quantitatively by calculating spatial averages for the terms appearing on the streamwise momentum budget equation.

3.1 Turbine layouts and simplification of the computational domain

The CFT pairs are set side-by-side with respect to the free stream. The two layouts that have been chosen for the pairs only differs for the turbine rotation verse, as shown in Fig. 3. We name "A-layout" the configuration in which the adjacent blades belonging to the two turbines move along with the wind inside the channel that separate them ("inner downwind" in [14]). We name "B- layout" the configuration with adjacent blades moving against the wind ("inner upwind" in [14]). To facilitate the understanding of the results, when we compare the behaviour of the two pairs to that of the single turbine, we will always show the turbine with positive rotation direction (the turbine in the pink box, in Fig. 3), i.e. counter-clockwise if viewed from above (positive z-axis).
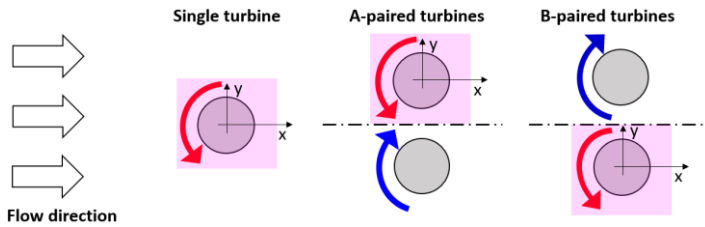

Fig. 3. Definitions for the rotation verse of the paired turbines in A and B layouts.

As in [14], the distance between the rotation axes is $1.3D$. Yet, to limit the cell number, half turbine is simulated. Doing this, the rotating and the fixed domains have about $6.8*10^6$ and $3.2*10^6$ hexahedral cells, respectively. Obviously, this simplification does not allow to take into account the significant effects of the proximity of the turbine to the floor of the test chamber [14] and, consequently, it will not be possible to make a direct comparison with the experimental results. Since simulating both turbines for such a number of revolutions as to guarantee almost complete development of the wake would be prohibitive even using supercomputers, the second crucial simplification of the computational domain was to limit the computations to just one of the two counter-rotating turbines, thereby assuming a symmetry plane between the pair. This is correct only if the vortices present in the wakes of the two turbines do not interpenetrate each other, however preliminary 2d simulations have shown that the flow field differences between the simulated half-domain and the simulated full-domain are negligible. In order to assume sufficiently stable the results at least at $6D$ downstream the turbine axis, 22 revolutions have been simulated. For further distances the wake is considered not completely developed and then the results are discarded.

3.2 Tip losses

In Fig. 4, on the left, the origin of the blade angular position (θ), and the "upwind" and "downwind" paths are recalled. On the right, the instantaneous C_P generated by the blade at $\mu=6\%$ during a revolution is reported, where μ is $z/(H/2)$, with the origin of z at the mid-span. At this span position, far from the blade tips, the typical behaviour that can also be found with 2d simulations can be well recognized [8, 9]. In fact, in upwind the power gain, due to more favourable attack angles, is allowed by a longer production duration (for A-layout the power production ends at larger θ, while for B-layout it starts at smaller c). In downwind the performance enhancement is significant for both the paired turbines, as allowed by the higher flow speeds induced by the wake contraction, due to the blockage exerted reciprocally by the two turbines. Moving towards the blade end, a C_P drop will occur as a consequence of tip losses, that consist in flow circulation over the tip occurring because of the pressure difference between the suction and the pressure sides of the blade [21].
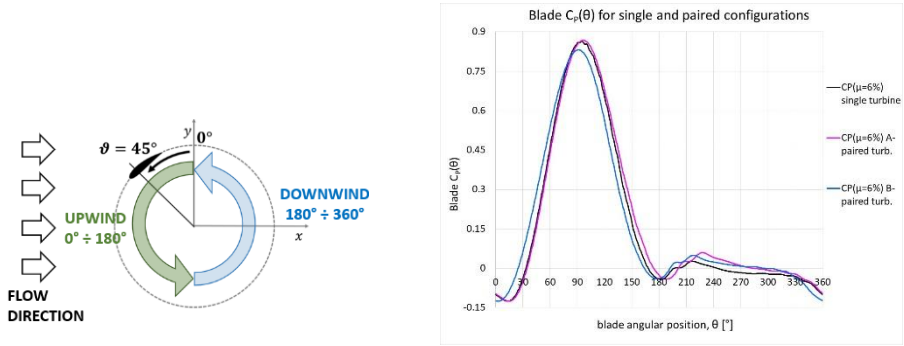
Fig. 4. (Left) Definitions for θ, and the upwind and downwind paths; (right) instantaneous C_P generated by the blade at μ=6% during a revolution.

As shown in Fig. 5 (on the left) depicting the span-wise distribution of the time-averaged C_P, despite for most of the blade length the performance of the paired layouts is better than that of the single turbine it drops early: for A-layout the $C_P(\mu)$ reaches the same value predicted for the single turbine at μ=94%, whereas for B-layout this happens even early, at μ=85%. The blade $C_P(\theta)$ diagram, corresponding to μ=96.7%, and shown in Fig. 5 (on the right) helps to understand way no advantageous effects are detectable for paired configurations in the final part of the blade length. It can be noticed that the mechanisms increasing the production in upwind still occur, however they are offset by a production decrease in downwind respect to the single turbine. This means that the wake contraction mechanism that should generate a performance improvement does not work near the blade tip.
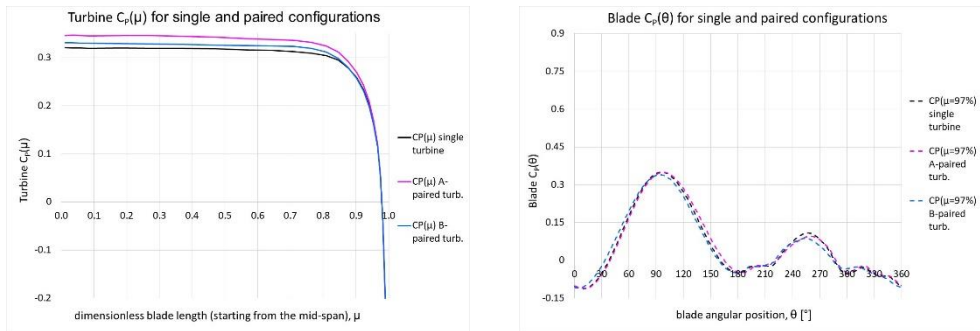

Fig. 5. (Left) Span-wise distribution of C_P, that is has time-averaged during the last revolution; (right) instantaneous C_P generated by the blade at μ=96.7% during a revolution.

To verify this, it is useful to analyse the streamwise velocity on a transversal plane set at a x corresponding to the passage of the blade at a θ for which a performance worsening is predicted, for instance θ=252° (x=0.476D), as shown in Fig. 6. The black frame shows the area swept by the of blade final 5%; the white dashed line shows the blade position at θ=252°; the dash-dot line remembers the side of the symmetry plane of the paired configurations. It can be seen that paired configurations entail higher flow velocity than in case of the isolated turbine for most of the region swept by the blades during downwind but not in proximity of the tips (black frame), especially close to the dashed line where the velocity is even slightly lower (yellow colour instead of the orange predicted for the single turbine). This, probably, indicates a lack of mutual blockage due to the end of the blades, similarly to the flow escape occurrence that generates the fluid dynamic losses at the tips. In spite of C_P increases, respect to the single turbine, of 8.0% and 3.1% calculated at the midspan for A and B layouts, the

overall increases were of 7.4% and 2.7% for A and B layouts. These gains are less of those measured by Vergaerde *et al.* [22], that were 14.2% and 15.9%, respectively.
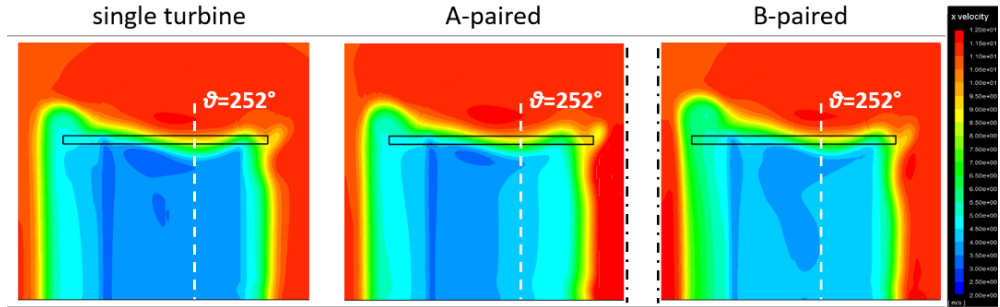

Fig. 6. Streamwise velocity for the single and the paired turbines on the transversal plane corresponding to the passage of the blade at θ=252° (the black frame indicates the final 5% of blade length).

3.3 Qualitative observations of the wake dynamics

In a recent paper, we evidenced that the large vortical structures visible in the near-wake of a CFT, and able to replenish the wake with high momentum flow, are the evolution of the dominant helical vortices shed at the blade tip, from which they also maintain the rotation direction (in particular, the sign of the x-vorticity) [13]. We have shown that the x-vorticity sign of tip vortices depends on which of the four quadrants swept by the blade (first and second halves of upwind, and first and second halves of downwind) they are released since, as the flow moves over the tip in a direction roughly perpendicular to the blade chord (the exact direction is determined by the pressure distribution on the blade profile), the chord slope respect to the free stream controls the sign of the x-vorticity. Therefore, the x-vorticity sign in the near-wake is determined by the quadrants where the strongest tip vortices are shed. For the turbine of the present study, since both the torque generation and the tip vortices are governed by the pressure difference between the suction and the pressure sides of the blade, the $C_P(\theta)$ diagram of Fig. 4 suggests that tip vortices are strong only in upwind. Fig. 7 depicts the x-vorticity distribution on the vertical plane passing through the blade tips. It can be noted that the x-vorticity is positive (red) for the first quadrant and negative (blue) for the second quadrant, and that the same signs characterize the near-wake x-vorticity. The figure also defines the windward and leeward sides of the wake respect to the turbine rotation direction.
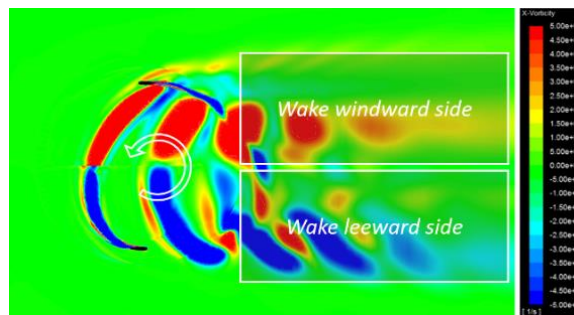

Fig. 7. *X*-vorticity on a horizontal plane at *z=H/2* for the single turbine (the blades are at θ=0° and 180°), together with the definitions of the wake windward and leeward sides.

Let's now analyse the wake evolution on transversal planes placed at 1*D*, 2.5*D*, 4*D* and 6*D* from the rotor axis as depicted in Fig. 8 and 9, respectively showing the cross-wise

velocity vectors and the streamwise velocity maps that have been time-averaged over the last two revolutions. The overlay added rectangular frame indicates the frontal size of the (half) turbine, moreover is must be specified that the observer is located upstream the turbine, therefore the windward side of the wake is on the left and the leeward side is on the right. We define "wake" the region characterised by a velocity deficit respect to U_0, therefore the region coloured by blue, green and yellow. U_0 corresponds to the orange, whereas the red region surrounding the wake indicates the high-momentum by-pass free stream which presence is crucial for the replenishment of the wake streamwise momentum.
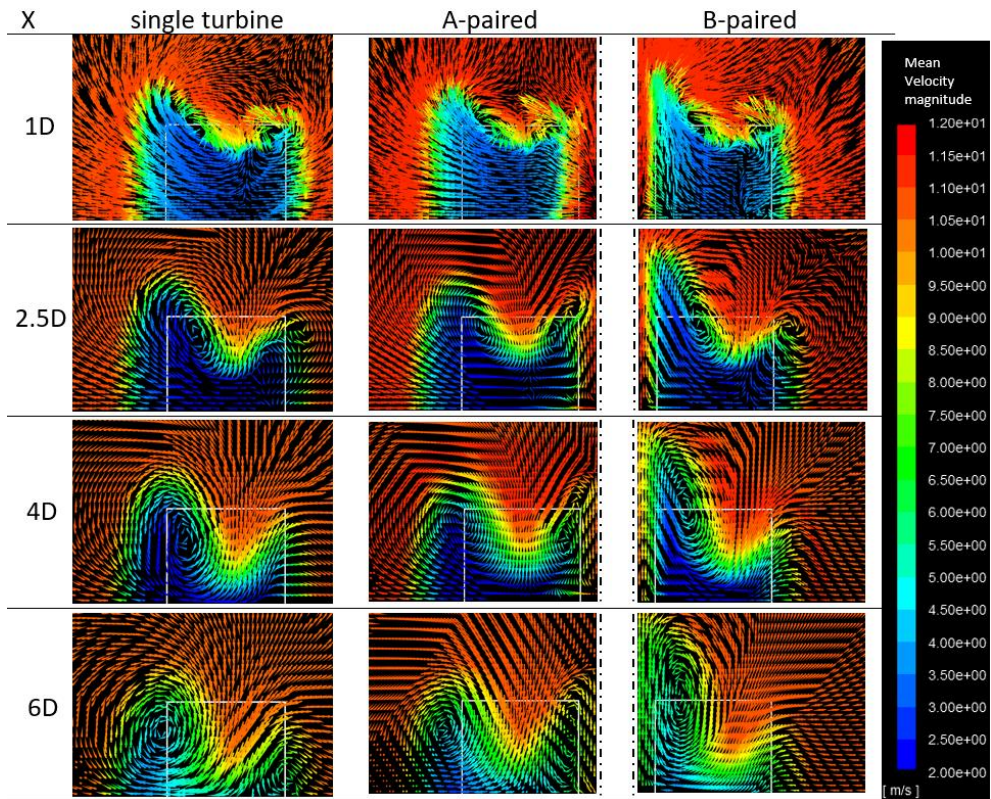

Fig. 8. Time-averaged cross-wise velocity vectors on transversal planes at $1D$, $2.5D$, $4D$ and $6D$ downstream the turbine axis, for single and paired turbines (coloured with velocity magnitude).

Let's start with the single CFT. We can see a pair of counter-rotating vortices at the turbine top boundary, which rotation verse is coherent with the tip vortices generated during the upwind passage of the blade. The vortex on the windward side is stronger and more shifted towards the region behind the turbine axis, in agreement with other studies concerning symmetrical [10, 11, 14] and camber-out [13] blade profiles. The rotation verses are such as to induce a massive vertical advection which reintroduces momentum into the top of the wake (well visible at x=2.5D); the asymmetrical characteristics of the vortices make the replenishment process asymmetrical as well, in fact at $6D$ the central and leeward parts of the wake appear almost completely re-energized. The two vortices imply not only vertical advection (advantageous at all distances), but also lateral advection, which on the windward side is always "negative" in the meaning that the flow moves from the heart towards the outside of the wake, with the result that the wake appears more and more enlarged to that side. On the leeward side, the lateral advection is negative only as long as the leeward weak vortex persists (i.e., up to 2.5D), in fact, since the vortex quickly disappears, the lateral

advection becomes "positive" as the flow enters the wake due to the action of the windward dominant vortex, which in the meantime has widened (albeit progressively getting weaker).

In case of the CFTs paired with A-layout, the wake evolves in a very similar manner, and at 6D the streamwise velocity distribution appears no much dissimilar from that of the single turbine, as visible in Fig. 9. The only differences are: a greater velocity deficit on the windward side, due to less lateral positive advection; a greater degree of re-energization near the plane of symmetry of the configuration, due to the presence inside the "channel" between the two CFTs of flow accelerated by the mutual blockage.

In case of B-layout the ever-positive vertical advection and the initially negative, then positive, leeward lateral advection appear similar to that seen for the single CFT, so much so that at 6D the shape and the degree of re-energization of the central and leeward parts of the wake are very similar to that of the isolated CFT. On the leeward side the wake appears even slightly more re-energized, due to a greater contribution by the lateral advection at 4D and 6D. However, the proximity of the symmetry plane to the dominant vortex prevents the wake from widening on the windward side and implies widening vertically. Consequently, at 6D the wake appears overall much more contracted in the horizontal direction and much higher in the vertical direction than in case of the single CFT. It should be noted that these main characteristics predicted for the wakes of A and B layouts agree with the experimental results by Vergaerde *et al.* [14].
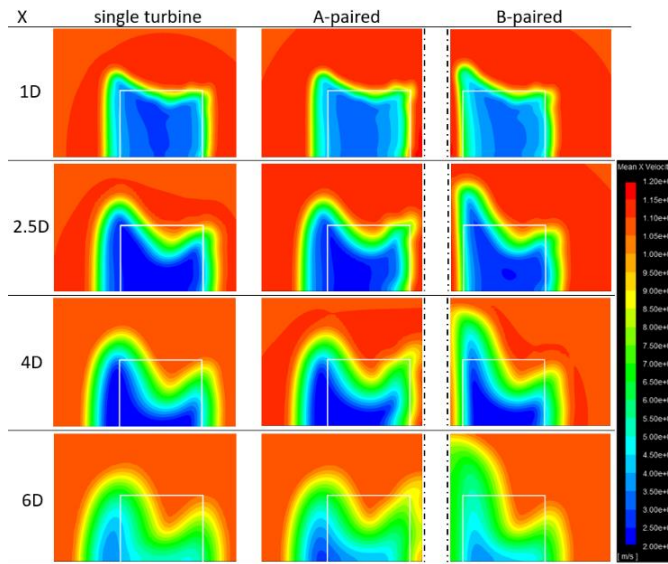

Fig. 9. Time-averaged streamwise velocity on transversal planes at 1D, 2.5D, 4D and 6D downstream the turbine axis, for single and paired turbines.

3.4 Analysis of the streamwise momentum budget

On the right hand of Eq. (1) there is the gradient of the streamwise velocity along *x*-axis, then a positive value means that the x-momentum is recovering while a negative value means that it is decreasing further. A positive value for a term on the right hand means that it is contributing to the wake recovery, for instance, a positive *y*-advection (or lateral advection) indicates that flow moving along the *y*-axis is entering the wake. Let's see how an important term on the right side which we have not yet discussed appears on transversal planes placed at 2.5D, 4D and 6D. Fig. 10 shows the *y*-turbulent transport term, that has been averaged over time and space as described in paragraph 2.2. In accordance with the literature [11], the

prevailing colour is red (i.e, positive contribution to the recovery) and the zones with the highest values are localized where strong velocity gradients occur, therefore at the boundaries of the wake. It is interesting to note that in paired CFTs an considerable increase of turbulent transport occurs at the wake side closer to the symmetry plane of the configuration, that is the leeward side and the windward side, respectively for A and B layouts. An aspect in line with the theory is that the turbulent mixing is a relatively "late" phenomenon, in that it is significant starting from the medium wake (see that at 4*D* and 6*D* it is higher than at 2.5*D*).
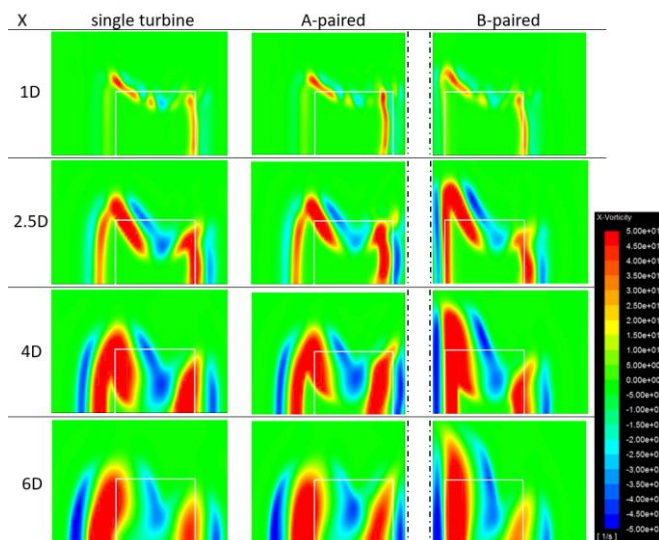

Fig. 10. Time-averaged values of the *y*-component of the turbulent transport on transversal planes at 1*D*, 2.5*D*, 4*D* and 6*D* downstream the turbine axis, for single and paired turbines.

The diagrams in Fig. 11 report the streamwise evolution for all the terms at the right hand of Eq. 1, and for their sum (i.e., the term at the left hand). It can be noted that the pressure transport term always remains negative, and its significant absolute value prevents the sum of all terms from becoming positive before 2.75*D*. Negative values for the pressure transport mean that the pressure is increasing and therefore inhibits the *x*-momentum recovery. This is intuitive, since the wake is characterized by low velocity and pressure and, moving away from the turbine, both the velocity and the pressure increase tending towards their freestream values. Although no comparisons can be found in literature as no one has shown the behaviour of this term in fully 3d studies, it is expected that in general this term does not give a positive contribution to the wake recovery. Other significant aspects noticeable in the diagrams are: the z-advection is the dominant mechanism of momentum recovery for single and paired CFTs, and it is positive already starting from the near-wake, while the y-advection is negative in the near-wake and became positive much later (after 4*D*); z-advection is lower in case of paired turbine; the y-turbulent transport is also significant starting from the medium-wake (after 3D), especially in case of B-layout, for which the y-turbulent transport is almost comparable to the z-advection; z-turbulent transport is less but quite relevant, whereas x-turbulent transport and viscous diffusion terms are negligible for all the cases. Afterwards, we summed the non-dimensional *x*, *y* and *z* components for the advection and for the turbulent transport, and reported the streamwise evolutions on the graph at the bottom-right in Fig. 11. It is evident that the overall advection is greater in case of single turbine for almost all the distances considered, and that both the overall advection and the overall turbulent transport better support the momentum recovery of B-layout than that of A-layout up to 5*D*.
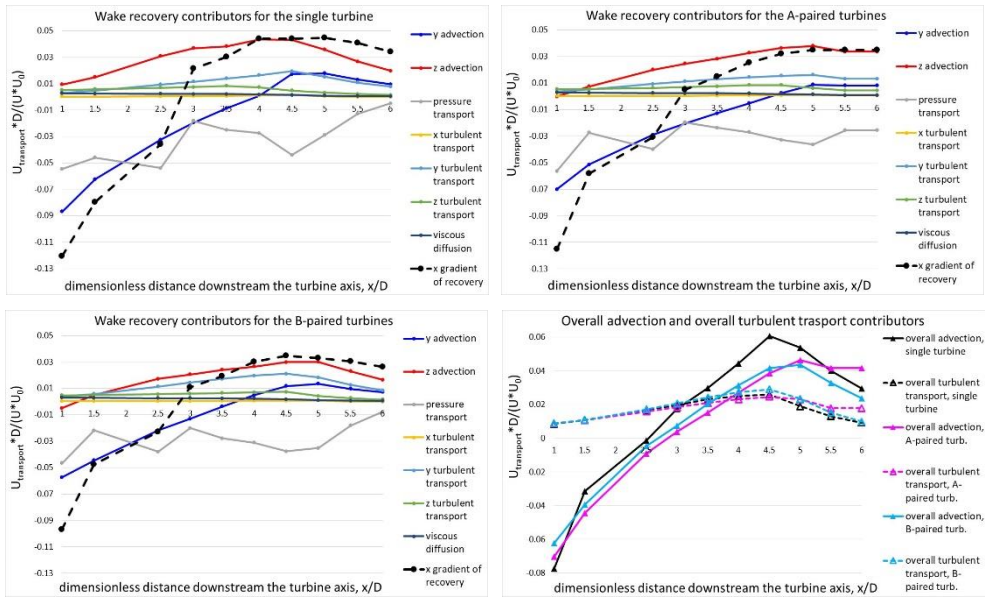
Fig. 11. Streamwise evolution of the non-dimensional cross-stream averages of all terms in Eq. (1) for single turbine (top-left), A-pair (top-right), and B-pair (bottom-left); streamwise evolution of the non-dimensional overall advection and overall turbulent transport (bottom-right).

The streamwise evolution of the most significant wake overall properties, that are the dimensionless U (as always, averaged on the wake transversal section) and the wake cross-sectional area are reported in Fig. 12. It is worth noting that, in comparison to the single turbine, at $6D$ the paired CFTs exhibit both a lower degree of velocity recovery and a less extended wake section. Since the wake section is continuously increasing, this simply means that the recovery is delayed, in other words, it will take longer distance to be complete. But, if we compare the A and B layouts, the latter is preferable to the former from the energetic point of view since, although for any distance there are no differences in U, the wake section for B-layout is lower, which means that the velocity deficit is less extensive.
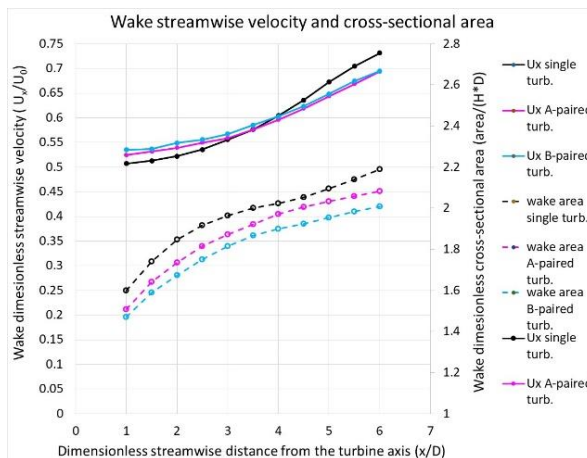

Fig. 12. Streamwise evolution of the dimensionless U (averaged on the wake transversal section) and of the wake cross-sectional area.

Conclusions

By means of 3d-CFD, we investigated the effects of the rotation verse of CFTs in paired counter-rotating configurations on the wake characteristics. The case study corresponds to the only experimental research found in literature and focusing on the wake behaviour of side-by-side CFTs pairs. We combined qualitative observations of the flow field with the momentum-budget approach, since it is useful to identify the fluid dynamic mechanisms which are effective in supporting wake recovery. Despite important domain simplifications that allowed to contain the calculation time, the wake results agree with experiments.

In the following the main finding.

- The counter-rotating vortex pairs occurring in the near-wake at the ends of the turbine, as a consequence of vortex shedding at the blade tips, promote the vertical advection that, entering high momentum flow inside the wake, is the main mechanism of wake replenishment.
- The wake characteristics greatly depend on the turbine rotation verse and then on the pairing layout; for A-layout (or "inner-downwind") the wake appears similar to that of a single turbine, whereas for B-layout (or "inner-upwind") it appears greatly contracted in horizontal direction and enlarged in vertical direction.
- For B-layout also the lateral advection gives a significant contribution to the momentum recovery.
- The contribution of the turbulent transport is less important, yet it becomes significant starting from the medium wake, especially for B-layout.
- The momentum recovery appears slightly more delayed than in case of a single turbine, yet, if we compare A and B layouts, the latter could be preferable to the former from the energetic point of view since its velocity deficit concerns a less extended wake cross-sectional area.

The wake characteristics could make B-layout preferable in case of farms based on staggered arrays, since by shortening the crosswise distances between adjacent pairs it could be possible to improve the farm power density. However, this study, which for the first time shows the C_P spanwise distribution of paired CFTs, also suggests that caution should be used in predicting the power gain resulting from the coupling of turbines as the tip losses are greater than in the case of an isolated turbine.

References

1. M. Borg, M. Collu, *A comparison between the dynamics of horizontal and vertical axis offshore floating wind turbines*, Philos. Trans. R. Soc. A Math. Phys. Eng. Sci. **373**. 20140076, (2015)

2. M. Borg, M. Collu, F. P. Brennan, *Offshore floating vertical Axis wind turbines: advantages, disadvantages, and dynamics modelling state of the art*, in: Mar. Offshore Renew. Energy (MORE 2012), 26-27 sept. (2012), London, UK

3. C. S. Ferreira, G. J. W. van Bussel, G. van Kuik, *An analytical method to predict the variation in performance of a H-Darrieus in skewed flow and its experimental validation*, in: Eur. Wind energy conf.; (2006)

4. A. Orlandi, M. Collu, S. Zanforlin, A. Shires, *3D URANS analysis of a vertical axis wind turbine in skewed flows*, J. Wind Engin. & Industrial Aerodyn. **147**:77-84, (2015). https://doi.org/10.1016/j.jweia.2015.09.010

5. J. O. Dabiri, *Potential order-of-magnitude enhancement of wind farm power density via counter-rotating vertical-axis wind turbine arrays*, J. Renew. Sustain. Energy **3**:43104, (2011)

6. M. Kinzel, Q. Mulligan, J. O. Dabiri*, Energy exchange in an array of vertical-axis wind turbines*, J. of Turbulence **13**, pp. 1-13, (2012)

7. I. D. Brownstein, N. J. Wei, J. O. Dabiri, *Aerodynamically Interacting Vertical-AxisWind Turbines: Performance Enhancement and Three-Dimensional Flow*, Energies **12**: 2724, (2019)

8. S. Zanforlin, T. Nishino, *Fluid dynamic mechanisms of enhanced power generation by closely spaced vertical axis wind turbines*, Renew. Energy **99**: 12 13-26, (2016)

9. S. Zanforlin, *Advantages of vertical axis tidal turbines set in close proximity: A comparative CFD investigation in the English Channel*, Ocean Engin. **156** 358–372, (2018)

10. P. Bachant, M. Wosnik, *Characterising the near-wake of a cross-flow turbine*, J. of Turbulence **16**(4):392-410, (2015)

11. V. F-C. Rolin, F. Porté-Agel, *Experimental investigation of vertical-axis wind-turbine wakes in boundary layer flow*, Renew. Energy **118**:1-13, (2018)

12. K. J. Ryan, F. Coletti, C. J. Elkins, J. O. Dabiri, J. K. Eaton, *Three-dimensional flow field around and downstream of a subscale model rotating vertical axis wind turbine*, Exp. Fluids **57**:38, (2016)

13. S. Zanforlin, P. Lupi, *Fluid Dynamic Mechanisms for the Wake Energy Recovery in Cross-Flow Turbines: Effects of Hydrofoil Shape and Turbine Solidity*. IX International Conference on Computational Methods in Marine Engineering, MARINE 2021, Edinburgh, Scotland, UK June 2-3 (2021)

14. A. Vergaerde, T. De Troyer, S. Muggiasca, I. Bayati, M. Belloli, J. Kluczewska-Bordier, N. Parneix, F. Silvert, M. C. Runacres, *Experimental characterisation of the wake behind paired vertical-axis wind turbines*, J. Wind Engin. & Industrial Aerodyn **206**:104353, (2020)

15. P. Ouro, S. Runge, Q. Luo, T. Stoesser, *Three-dimensionality of the wake recovery behind a vertical axis turbine*, Renew. Energy **133**:1066-1077, (2019)

16. A. Posa, *Dependence of the wake recovery downstream of a Vertical Axis Wind Turbine on its dynamic solidity*. J. Wind Engin. & Industrial Aerodyn. **202**:104212, (2020)

17. T. Maître, E. Amet, C. Pellone, *Modeling of the flow in a Darrieus water turbine: Wall grid refinement analysis and comparison with experiments*, Renew. Energy **51**:497–512, (2013)

18. F. R. Menter, *Two-equation eddy-viscosity turbulence models for engineering applications*, AIAA J. **32**:1598–1605, (1994)

19. D. C. Wilcox, *Formulation of the k-ω turbulence model revisited*, AIAA J. **46**:2823–2838, (2008)

20. F. Balduzzi, A. Bianchini, R. Maleci, G. Ferrara, L. Ferrari, *Critical issues in the CFD simulation of Darrieus wind turbines*, Renew. Energy **85**:419–435, (2016)

21. S. Zanforlin, S. Deluca, *Effects of the Reynolds number and the tip losses on the optimal aspect ratio of straight-bladed Vertical Axis Wind Turbines*, Energy **148**:179-195, (2018)

22. A. Vergaerde, T. De Troyer, L. Standaert, J. Kluczewska-Bordier, D. Pitance, A. Immas, F. Silvert, M.C. Runacres, *Experimental validation of the power enhancement of a pair of vertical-axis wind turbines*, Renewable Energy **146**:181-187 (2020)